

Searches for neutrinos in the direction of radio-bright blazars with the ANTARES telescope

ANTARES Collaboration: A. Albert^{1,2}, S. Alves³, M. André⁴, M. Ardid⁵, and S. Ardid⁵, J.-J. Aubert⁶, J. Aublin^{*7}, B. Baret⁷, S. Basa⁸, Y. Becherini⁷, B. Belhorma⁹, M. Bendahman^{7,10}, F. Benfenati^{11,12}, V. Bertin⁶, S. Biagi¹³, M. Bissinger¹⁴, J. Boumaaza¹⁰, M. Bouta¹⁵, M.C. Bouwhuis¹⁶, H. Brânzaș¹⁷, R. Bruijn^{16,18}, J. Brunner⁶, J. Busto⁶, B. Caiiffi¹⁹, D. Calvo³, S. Champion^{20,21}, A. Capone^{20,21}, L. Caramete¹⁷, F. Carenini^{11,12}, J. Carr⁶, V. Carretero³, S. Celli^{20,21}, L. Cerisy⁶, M. Chabab²², R. Cherkaoui El Moursli¹⁰, T. Chiarusi¹¹, M. Circella²³, J.A.B. Coelho⁷, A. Coleiro⁷, R. Coniglione¹³, P. Coyle⁶, A. Creusot⁷, A.S.M. Cruz²⁴, A. F. Díaz²⁵, B. De Martino⁶, C. Distefano¹³, I. Di Palma^{20,21}, A. Domi^{16,18}, C. Donzaud^{7,26}, D. Dornic⁶, D. Drouhin^{1,2}, T. Eberl¹⁴, T. van Eeden¹⁶, D. van Eijk¹⁶, S. El Hedri⁷, N. El Khayati¹⁰, A. Enzenhöfer⁶, P. Fermani^{20,21}, G. Ferrara¹³, F. Filippini^{11,12}, L. Fusco²⁷, S. Gagliardini^{20,21}, J. García⁵, C. Gatiús Oliver¹⁶, P. Gay^{28,7}, N. Geißelbrecht¹⁴, H. Glotin²⁹, R. Gozzini³, R. Gracia Ruiz¹⁴, K. Graf¹⁴, C. Guidi^{19,30}, L. Haegel⁷, S. Hallmann¹⁴, H. van Haren³¹, A.J. Heijboer¹⁶, Y. Hello³², J.J. Hernández-Rey³, J. Höbl¹⁴, J. Hofestädt¹⁴, F. Huang⁶, G. Illuminati^{†11}, C. W. James²⁴, B. Jisse-Jung¹⁶, M. de Jong^{16,33}, P. de Jong^{16,18}, M. Kadler³⁴, O. Kalekin¹⁴, U. Katz¹⁴, A. Kouchner⁷, I. Kreykenbohm³⁵, V. Kulikovskiy¹⁹, R. Lahmann¹⁴, M. Lamoureux⁷, A. Lazo³, D. Lefèvre³⁶, E. Leonora³⁷, G. Levi^{11,12}, S. Le Stum⁶, D. Lopez-Coto³⁸, S. Loucatos^{39,7}, L. Maderer⁷, J. Manczak³, M. Marcellin⁸, A. Margiotta^{11,12}, A. Marinelli^{42,43}, J.A. Martínez-Mora⁵, P. Migliozzi⁴⁰, A. Moussa¹⁵, R. Muller¹⁶, S. Navas³⁸, E. Nezri⁸, B. Ó Fearraigh¹⁶, E. Oukacha⁷, A. Păun¹⁷, G.E. Păvălaș¹⁷, S. Peña-Martínez⁷, M. Perrin-Terrin⁶, V. Pestel¹⁶, P. Piattelli¹³, C. Poirè⁵, V. Popa¹⁷, T. Pradier¹, N. Randazzo³⁷, D. Real³, S. Reck¹⁴, G. Riccobene¹³, A. Romanov^{19,30}, A. Sánchez-Losa^{3,23}, A. Saina³, F. Salesa Greus³, D. F. E. Samtleben^{16,33}, M. Sanguineti^{19,30}, P. Sapienza¹³, J. Schnabel¹⁴, J. Schumann¹⁴, F. Schüssler³⁹, J. Seneca¹⁶, M. Spurio^{11,12}, Th. Stolarczyk³⁹, M. Taiuti^{19,30}, Y. Tayalati¹⁰, S.J. Tingay²⁴, B. Vallage^{39,7}, G. Vannoye⁶, V. Van Elewyck^{7,41}, S. Viola¹³, D. Vivolo^{40,44}, J. Wilms³⁵, S. Zavatarelli¹⁹, A. Zegarelli^{20,21}, J.D. Zornoza³, and J. Zúñiga³

Y. A. Kovalev^{45,a}, Y. Y. Kovalev^{46,45,47,a}, A. V. Plavin^{†48,45,a},
A. B. Pushkarev^{49,45,a}, and S. V. Troitsky^{50,51,a}

OVRO Collaboration: T. Hovatta^{52,53}, S. Kiehlmann^{54,55}, I. Liodakis⁵², V.

Pavlidou^{54,55}, and A.C.S Readhead⁵⁶

- ¹Université de Strasbourg, CNRS, IPHC UMR 7178, F-67000 Strasbourg, France
²Université de Haute Alsace, F-68100 Mulhouse, France
³IFIC - Instituto de Física Corpuscular (CSIC - Universitat de València) c/ Catedrático José Beltrán, 2 E-46980 Paterna, Valencia, Spain
⁴Technical University of Catalonia, Laboratory of Applied Bioacoustics, Rambla Exposició, 08800 Vilanova i la Geltrú, Barcelona, Spain
⁵Institut d'Investigació per a la Gestió Integrada de les Zones Costaneres (IGIC) - Universitat Politècnica de València. C/ Paraninf 1, 46730 Gandia, Spain
⁶Aix Marseille Univ, CNRS/IN2P3, CPPM, Marseille, France
⁷Université Paris Cité, CNRS, Astroparticule et Cosmologie, F-75013 Paris, France
⁸Aix Marseille Univ, CNRS, CNES, LAM, Marseille, France
⁹National Center for Energy Sciences and Nuclear Techniques, B.P.1382, R. P.10001 Rabat, Morocco
¹⁰University Mohammed V in Rabat, Faculty of Sciences, 4 av. Ibn Battouta, B.P. 1014, R.P. 10000
¹¹INFN - Sezione di Bologna, Viale Berti-Pichat 6/2, 40127 Bologna, Italy
¹²Dipartimento di Fisica e Astronomia dell'Università di Bologna, Viale Berti-Pichat 6/2, 40127, Bologna, Italy
¹³INFN - Laboratori Nazionali del Sud (LNS), Via S. Sofia 62, 95123 Catania, Italy
¹⁴Friedrich-Alexander-Universität Erlangen-Nürnberg, Erlangen Centre for Astroparticle Physics, Erwin-Rommel-Str. 1, 91058 Erlangen, Germany
¹⁵University Mohammed I, Laboratory of Physics of Matter and Radiations, B.P.717, Oujda 6000, Morocco
¹⁶Nikhef, Science Park, Amsterdam, The Netherlands
¹⁷Institute of Space Science, RO-077125 Bucharest, Măgurele, Romania
¹⁸Universiteit van Amsterdam, Instituut voor Hoge-Energie Fysica, Science Park 105, 1098 XG Amsterdam, The Netherlands
¹⁹INFN - Sezione di Genova, Via Dodecaneso 33, 16146 Genova, Italy
²⁰INFN - Sezione di Roma, P.le Aldo Moro 2, 00185 Roma, Italy
²¹Dipartimento di Fisica dell'Università La Sapienza, P.le Aldo Moro 2, 00185 Roma, Italy
²²LPHEA, Faculty of Science - Semlali, Cadi Ayyad University, P.O.B. 2390, Marrakech, Morocco.
²³INFN - Sezione di Bari, Via E. Orabona 4, 70126 Bari, Italy
²⁴International Centre for Radio Astronomy Research - Curtin University, Bentley, WA 6102, Australia
²⁵Department of Computer Architecture and Technology/CITIC, University of Granada, 18071 Granada, Spain
²⁶Université Paris-Sud, 91405 Orsay Cedex, France
²⁷Università di Salerno e INFN Gruppo Collegato di Salerno, Dipartimento di Fisica, Via Giovanni Paolo II 132, Fisciano, 84084 Italy
²⁸Laboratoire de Physique Corpusculaire, Clermont Université, Université Blaise Pascal, CNRS/IN2P3, BP 10448, F-63000 Clermont-Ferrand, France
²⁹LIS, UMR Université de Toulon, Aix Marseille Université, CNRS, 83041 Toulon, France
³⁰Dipartimento di Fisica dell'Università, Via Dodecaneso 33, 16146 Genova, Italy
³¹Royal Netherlands Institute for Sea Research (NIOZ), Landsdiep 4, 1797 SZ 't Horntje (Texel), the Netherlands
³²Géoazur, UCA, CNRS, IRD, Observatoire de la Côte d'Azur, Sophia Antipolis, France
³³Huygens-Kamerlingh Onnes Laboratorium, Universiteit Leiden, The Netherlands
³⁴Institut für Theoretische Physik und Astrophysik, Universität Würzburg, Emil-Fischer Str. 31, 97074 Würzburg, Germany
³⁵Dr. Reimis-Sternwarte and ECAP, Friedrich-Alexander-Universität Erlangen-Nürnberg, Sternwartstr. 7, 96049 Bamberg, Germany
³⁶Mediterranean Institute of Oceanography (MIO), Aix-Marseille University, 13288, Marseille, Cedex 9, France; Université du Sud Toulon-Var, CNRS-INSU/IRD UM 110, 83957, La Garde Cedex, France
³⁷INFN - Sezione di Catania, Via S. Sofia 64, 95123 Catania, Italy
³⁸Dpto. de Física Teórica y del Cosmos & C.A.F.P.E., University of Granada, 18071 Granada, Spain
³⁹IRFU, CEA, Université Paris-Saclay, F-91191 Gif-sur-Yvette, France
⁴⁰INFN - Sezione di Napoli, Via Cintia 80126 Napoli, Italy
⁴¹Institut Universitaire de France, 75005 Paris, France
⁴²Dipartimento di Fisica Ettore Pancini, Università degli studi di Napoli Federico II, Complesso Univ. Monte S. Angelo, I-80126 Napoli, Italy
⁴³INFN - Sezione di Napoli, Complesso Univ. Monte S. Angelo, I-80126 Napoli, Italy
⁴⁴Dipartimento di Fisica dell'Università Federico II di Napoli, Via Cintia 80126, Napoli, Italy
⁴⁵Lebedev Physical Institute of the Russian Academy of Sciences, Leninsky prospekt 53, 119991 Moscow, Russia
⁴⁶Max-Planck-Institut für Radioastronomie, Auf dem Hügel 69, 53121 Bonn, Germany
⁴⁷Moscow Institute of Physics and Technology, Institutsky per. 9, Dolgoprudny 141700, Russia
⁴⁸Black Hole Initiative at Harvard University, 20 Garden Street, Cambridge, MA 02138, USA
⁴⁹Crimean Astrophysical Observatory, 298409 Nauchny, Crimea, Russia
⁵⁰Institute for Nuclear Research of the Russian Academy of Sciences, 60th October Anniversary Prospect 7a, Moscow, Russia
⁵¹Faculty of Physics, M.V. Lomonosov Moscow State University, 1-2 Leninskie Gory, Moscow 119991, Russia
⁵²Finnish Center for Astronomy with ESO, University of Turku, Vesilinnantie 5, FI-20014, Finland
⁵³Aalto University Metsähovi Radio Observatory, Metsähovintie 114, FI-02540 Kylmäla, Finland
⁵⁴Institute of Astrophysics, Foundation for Research and Technology-Hellas, GR-70013 Heraklion, Greece
⁵⁵Department of Physics and Institute of Theoretical and Computational Physics, University of Crete, 70013 Heraklion, Greece
⁵⁶Owens Valley Radio Observatory, California Institute of Technology, Pasadena, CA 91125, USA

^aThe shown author affiliations reflect their job contracts; the ANTARES collaboration has currently suspended all

Abstract

Active galaxies, especially blazars, are among the most promising neutrino source candidates. To date, ANTARES searches for these objects considered GeV-TeV γ -ray bright blazars. Here, a statistically complete radio-bright blazar sample is used as the target for searches of origins of neutrinos collected by the ANTARES neutrino telescope over 13 years of operation. The hypothesis of a neutrino-blazar directional correlation is tested by pair counting and by a complementary likelihood-based approach. The resulting post-trial p -value is 3.0% (2.2σ in the two-sided convention), possibly indicating a correlation. Additionally, a time-dependent analysis is performed to search for temporal clustering of neutrino candidates as a mean of detecting neutrino flares in blazars. None of the investigated sources alone reaches a significant flare detection level. However, the presence of 18 sources with a pre-trial significance above 3σ indicates a $p = 1.4\%$ (2.5σ in the two-sided convention) detection of a time-variable neutrino flux. An *a posteriori* investigation reveals an intriguing temporal coincidence of neutrino, radio, and γ -ray flares of the J0242+1101 blazar at a $p = 0.5\%$ (2.9σ in the two-sided convention) level. Altogether, the results presented here suggest a possible connection of neutrino candidates detected by the ANTARES telescope with radio-bright blazars.

1 Introduction

Astrophysical neutrinos of high energies were discovered almost ten years ago by the IceCube Collaboration [1], consistently with later studies with the other two existing instruments, namely ANTARES [2] and Baikal-GVD [3]. However, their origin is still not fully determined. Observational evidence exists for a wide range of neutrino sources, including individual active galaxies [4, 5, 6], large samples of blazars [7, 8, 9, 10, 11, 12, 13, 14], and the Milky Way Galaxy [15, 16, 17, 18, 19, 20, 21].

Active galaxies, and particularly blazars, which have their jets pointed towards us, form a very promising class of neutrino source candidates [22, 23, 24, 25]. The emission from the jet is detectable across cosmological distances thanks to the relativistic beaming [26]. Similar beaming effects should affect neutrinos as well, enhancing their chance to be detected on Earth. Moreover, there are hints that neutrinos are predominantly produced during major flares close to the jet origin [7, 27], indicating a tight physical connection between jets and neutrino production processes.

Currently, all associations of high-energy neutrinos with celestial objects or classes thereof are fundamentally statistical. The comparison of findings based on different instruments is crucial to understand both astrophysical neutrino flux characteristics, such as its energy spectrum, and potential systematic effects inherent to their detection. Earlier searches for a neutrino signal in the ANTARES detector from the direction of blazars were performed using γ -bright blazars contained in the *Fermi* LAT catalog [28, 29]. However, recent studies suggest that emission and flares in γ -rays may not be tightly correlated with neutrino sources [30, 8, 31]: hadronic γ -rays are co-produced together with neutrinos, but quickly cascade down in energy. Synchrotron

*Corresponding author

†Corresponding author

‡Corresponding author

emission from blazar jets, detected on Earth as radio emission, could likely be a better tracer of relativistic beaming and activity happening close to the jet origin.

In addition, the recent publication of the IceCube Event Catalog of Alert Tracks-1 [32], containing a revised sample of neutrino candidates with a high probability of being of astrophysical origin, has been followed by a search [33] for a correlation with the population of blazars contained in the *Fermi* 4LAC-DR2 catalog [34] and in the Radio Fundamental Catalog¹. As no significant correlation is found, this result mitigates the previous findings of [7], and indicates that only a minority of the γ -ray bright and radio-bright AGN population can be identified as potential sources of high-energy neutrinos.

This paper presents an independent and complementary study of the possible neutrino-blazar association with data collected by the ANTARES observatory. Section 2 and Section 3 define the dataset used in the analysis: the ANTARES neutrino candidates and the radio observations of inner blazar regions. A description of the employed analysis methods and respective results follows. The hypothesis of directional correlation between neutrinos and blazar emission is tested by mean of a neutrino-blazar pair counting method (Section 4), as well as of a complementary time-integrated likelihood-based approach (Section 5). Moreover, in order to search for a time clustering of ANTARES events coming from the blazar directions, a time-dependent likelihood scan is also performed (Section 6). In Section 7, the results of a follow-up search for multi-messenger time flare associations are presented. Finally, Section 8 summarizes all findings and discusses further prospects.

2 ANTARES detector and data sample

ANTARES [35] was an undersea high-energy neutrino telescope, located 40 km off-shore from Toulon, France, below the surface of the Mediterranean Sea. After over 15 years of operation, it took its last data in February 2022. The detector consisted of a three-dimensional array of 885 photomultiplier tubes (PMTs), distributed along 12 vertical lines of 450 m length, for a total instrumented volume of $\sim 0.01 \text{ km}^3$. Each line was anchored to the seabed at a depth of about 2500 m and held taut by a buoy at the top. The PMTs collected the Cherenkov photons induced by the passage of the relativistic charged particles produced in neutrino interactions inside or near the instrumented volume. The information provided by the position, time and collected charge of the signals in the PMTs can be used to infer the direction and energy of the incident neutrino.

Two main event topologies, induced by different neutrino flavours and types of interactions, could be identified: track-like and shower-like events. Charged current (CC) interactions of muon neutrinos produce relativistic muons that can travel large distances through the medium, with Cherenkov light being induced all along the muon path, resulting in a track-like signature in the detector. The parent neutrino direction of high-quality selected tracks can be reconstructed with a median angular resolution of $\sim 0.8^\circ$ at $E_\nu \sim 1 \text{ TeV}$ and below $\sim 0.4^\circ$ for $E_\nu > 10 \text{ TeV}$ [36] thanks to the long lever arm of this channel. Shower-like events are induced by all-flavour neutral current (NC) as well as ν_e and ν_τ CC interactions. This topology is characterised by an almost spherical light emission around the shower maximum, with an elongation of a few metres, which results in a worse estimation of the parent neutrino direction compared to the track channel. A median angular resolution of $\sim 3^\circ$ is achieved for high-quality selected showers with energies between 1 TeV and 0.5 PeV [36].

The data set employed in this analysis includes events recorded in ANTARES between January 29, 2007 and February 29, 2020 (3845 days of livetime), and selected using the criteria

¹<http://astrogeo.smce.nasa.gov/rfc/>

defined in [36], optimized to minimise the neutrino flux needed for a 5σ discovery of a point-like source with a $\propto E^{-2.0}$ emission spectrum. The selection includes cuts on the zenith angle, the angular error estimate and parameters describing the quality of the reconstruction. In the shower channel, an additional cut is applied on the interaction vertex, required to be located within a fiducial volume slightly larger than the instrumented volume. Recently improved calibrations have been used to reconstruct all the selected ANTARES events. This yields slightly different values of the reconstructed direction – with $\sim 98\%$ of the selected events being reconstructed within 1° from the previous direction – and of the quality parameters associated with each event. In addition, the estimator of the energy for track-like events has been updated, taking into account the time-evolution of the detector over the whole data-taking period. A total of 10504 track-like and 227 shower-like events survive the selection, with an expected atmospheric muon contamination of $\sim 14\%$ and $\sim 43\%$ for the track and the shower channel, respectively. Only the track channel is employed in the search for directional correlations, while the search for neutrino temporal flares makes use of both tracks and showers.

3 Radio observations of blazars

Synchrotron emission from inner regions of blazar jets is observed and measured by radio telescopes using very long baseline interferometry (VLBI) techniques. VLBI-measured flux densities represent the emission from the very central parsecs of blazars, and these measurements are used to select the objects included in this analysis.

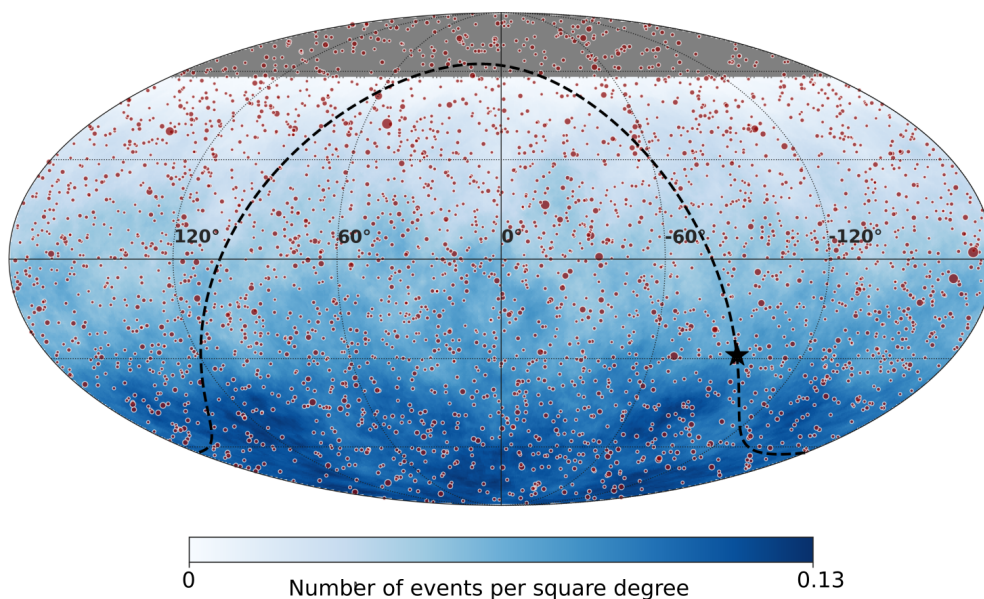


Figure 1: Equatorial sky map showing the location of the VLBI blazars (red dots), together with the average density of ANTARES track-like and shower-like events per square degree. The event density at a given point in the sky is obtained dividing the number of events found within a cone of 10° radius around this point by the solid angle of the cone. The surface of the markers is proportional to the VLBI 8 GHz flux density. The blazars located in the grey region at high declinations are outside the ANTARES field of view. The dashed black line shows the Galactic plane, and the Galactic center is represented as a black star marker.

A complete flux-limited sample of blazars observed by VLBI is selected using the same criteria as in [8]. Accurate positions and parsec-scale flux densities of observed blazars are compiled in the Radio Fundamental Catalogue². Observations at 8 GHz are utilized because of their completeness across the whole sky. There are 3411 blazars with historical average flux density above 150 mJy; 3051 of them fall into the ANTARES field of view and are targeted by the searches for directional correlations. Figure 1 shows the location of the selected blazars in equatorial coordinates, together with the ANTARES neutrino candidates. As for the time-dependent scan, the sources with low visibility, i.e. located above 40° in declination, are excluded from the search, leading to a targeted catalog of 2774 blazars. The collection of observations includes geodetic VLBI [37, 38, 39], the Very Long Baseline Array (VLBA) calibrator surveys (VCS [40, 41, 42, 43, 44, 45, 46, 47]), other 8 GHz global VLBI, VLBA, EVN (the European VLBI Network) and LBA (the Australian Long Baseline Array) programs [48, 49, 50, 51, 52, 53, 54, 55].

4 Counting method

The first correlation analysis uses a simple method, inspired by [7], where the observable is the number of neutrino-blazar angular pairs separated by an angular distance Ψ less than $x \cdot \beta$. Here, β is the angular uncertainty coming from the neutrino reconstruction, and x is a free parameter that varies in the interval $[0.1; 2]$. The parameter x is meant to take into account a possible systematic difference between the output of the reconstruction algorithm and the true (unknown) angular error radius. Using Monte Carlo simulations, the relationship between the error estimate β and the true 68% containment radius $\Psi_{68\%}$ can be assessed. For values $\beta \lesssim 0.5$, and reconstructed energies above ~ 10 TeV, the relation between β and $\Psi_{68\%}$ is close to what is expected from a two-dimensional Gaussian function. At lower energies and for higher values of β , the value of $\Psi_{68\%}$ becomes significantly higher than the Gaussian expectation. The scan on the x parameter is then an empirical way to take into account this complicated behavior while still using the reconstruction quality information of ANTARES neutrinos on an event-by-event basis. As a consequence, the p -value obtained with this method needs a trial factor correction.

A possible correlation between the radio-flux density and neutrino emission is evaluated by performing an additional scan on the radio-flux density $S_{8\text{GHz}}$: VLBI blazars are kept in the sample if they satisfy $S_{8\text{GHz}} > S_{\text{min}}$, and the value of S_{min} is varied in the range $[0.15; 5]$ Jy.

The results of the counting analysis are illustrated in Figures 2 and 3. When using the full VLBI catalog, the one-dimensional scan shows an absolute minimum for $x = 0.82$, where $n_{\text{obs}} = 469$ pairs are observed in data, while $n_{\text{exp}} = 410.4$ are expected on average from random simulations (59 pairs in excess). The associated pre-trial p -value is $p = 2.5 \times 10^{-3}$ (3.0σ), leading after correction to a post-trial p -value of $P = 3.0 \times 10^{-2}$ (2.2σ). Note that without performing a scan, the value $p(x = 1) = 5.0 \times 10^{-2}$ (2.0σ) would have been quoted instead.

The position $x = 0.82$ of the minimum seems to indicate that the angular uncertainty β of the neutrinos is over-estimated, which is not what is expected from Monte Carlo. However, the position of this scan minimum is subject to random fluctuations, and as the excess is not statistically significant, this observation cannot be interpreted as evidence for an issue in the ANTARES track reconstruction.

The search for a correlation with radio flux density with the two-dimensional scan (x, S_{min}) is shown in Figure 3. The absolute minimum is found for $x = 0.82$ and $S_{\text{min}} = 0.15$ Jy, with a pre-trial p -value of $p(S > 0.15 \text{ Jy}) = 2.5 \times 10^{-3}$, and a post-trial $P(S > 0.15 \text{ Jy}) = 0.26$. This minimum corresponds to the previous findings of the one dimensional scan, and is obtained for the lowest value of the flux density cut, meaning that the whole VLBI blazar catalog is included.

²http://astrogeo.smce.nasa.gov/sol/rfc/rfc_2020d/

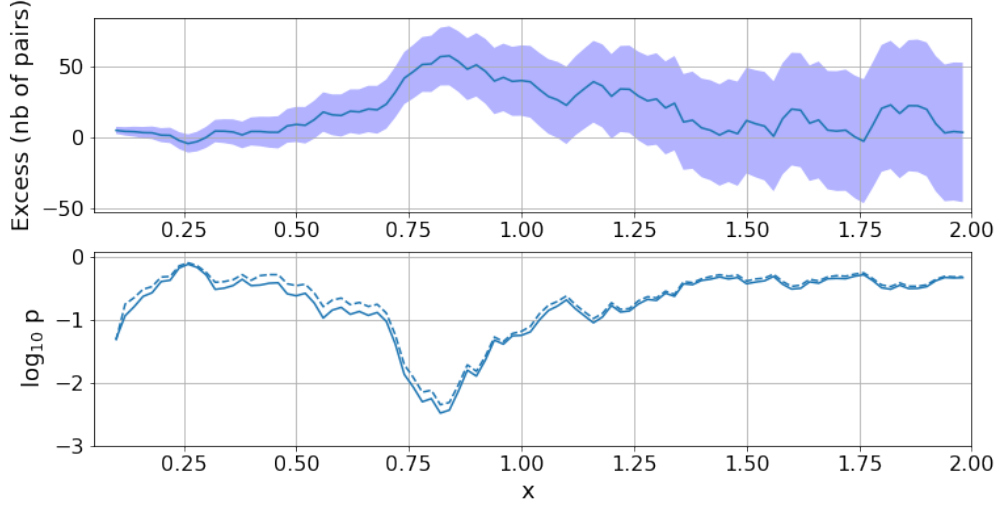


Figure 2: Result of the counting analysis with the VLBI blazar catalog. The top and bottom panels show, as a function of the parameter x (defined in the text), the observed excess of pairs relative to random expectations, and the pre-trial p -value respectively. In the top panel, the blue band shows the $\pm 1\sigma$ confidence interval. In the bottom panel, the dashed curve shows the p -value obtained when excluding blazars with $S > 3.68$ Jy from the catalog.

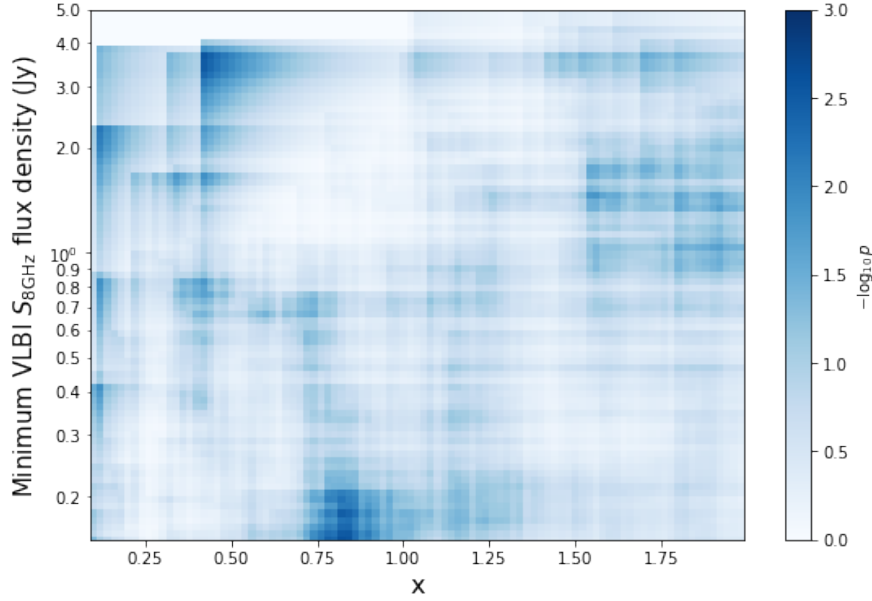


Figure 3: Result of the two-dimensional scan over the radio-flux density $S_{8\text{GHz}}$ and parameter x . The color code indicates the pre-trial p -value.

A local minimum is also visible for $x = 0.42$ and $S_{\text{min}} = 3.68$ Jy, with a pre-trial p -value of $p(S > 3.68 \text{ Jy}) = 2.7 \times 10^{-3}$. This excess is mainly driven by 3 blazars: J0609–1542 and

J1743–0350, that have one very close ANTARES track (less than 0.2° away), and J0538–4405 that has two events at 0.4° distance. These sources are not found in the search for neutrino flares presented in Section 6, as only one neutrino is contributing for J0609–1542 and J1743–0350, and the two events located around J0538–4405 are separated by more than 6.5 years in time.

When accounting for the trial factors, the significance of this excess is $P(S > 3.68 \text{ Jy}) = 0.28$. In addition, as can be seen in Figure 2 (dashed line), when excluding the blazars with $S > 3.68 \text{ Jy}$ from the catalog, the position of the minimum stays the same, and the pre-trial p -value is only slightly increased $p = 4.5 \times 10^{-3}$. These results indicate that the excess in the counting of neutrinos-blazar pairs is not induced by a small number of very high flux sources in the VLBI catalog.

5 Time-integrated likelihood analysis

A time-integrated likelihood analysis very similar to the one reported in [29] is performed, making use of more information about the ANTARES detector response than the one used in the simple counting method. The likelihood of the null hypothesis H_b where only background is present is compared with an alternative hypothesis H_{s+b} where signal events coming from blazars are present in the data.

The neutrino signal events are assumed to come from blazars in proportion to their measured VLBI flux density $S_{8\text{GHz}}$, with an energy spectrum modeled as a pure power-law $E^{-\gamma}$. The analysis is performed for a fixed value of the spectral index γ , and repeated for values $\gamma \in [1.8; 2.6]$ in 0.1 steps.

The likelihood is written as:

$$\ln \mathcal{L}_{s+b} = \sum_i^N \ln (\mu_s S_i + \mu_b B_i) - \mu_s - \mu_b, \quad (1)$$

where N is the total number of observed track-like events, S_i is the probability density function (PDF) of the signal and B_i the background one. The free parameters are the estimated number of signal μ_s and background μ_b events. The expression of the background-only likelihood \mathcal{L}_b is simply obtained by setting $\mu_s = 0$ in Equation 1.

The test statistics Q is defined as a likelihood ratio:

$$Q = 2 \ln \left[\frac{\max(\mathcal{L}_{s+b})}{\max(\mathcal{L}_b)} \right], \quad (2)$$

where the likelihoods defined in Equation 1 are maximized with respect to the free parameters μ_s and μ_b . In practice, as the background-only term \mathcal{L}_b is maximal when $\mu_b = N$, the numerical procedure of likelihood maximization has to be performed only for the \mathcal{L}_{s+b} term.

The core ingredients of the likelihood analysis are the signal and background PDF, which are written as the product of a spatial and an energy term:

$$S_i = f_s(\alpha_i, \delta_i, \beta_i, E_i) g_s(E_i) \quad \text{and} \quad B_i = f_b(\delta_i, E_i) g_b(E_i), \quad (3)$$

where (α_i, δ_i) are the equatorial coordinates, β_i the angular uncertainty and E_i the estimated energy of the i^{th} neutrino candidate.

The energy-dependent part of the signal PDF, $g_s(E)$, is computed using Monte Carlo simulations, by building a histogram of the reconstructed energies E of track-like events when assuming a pure power-law $E_{\text{true}}^{-\gamma}$ distribution of the true neutrino energies E_{true} . The background PDF,

$g_b(E)$, is similarly obtained by building a histogram with Monte Carlo simulations, where the atmospheric neutrino fluxes (conventional+prompt components) and atmospheric muons fluxes are taken into account (see [56] for details).

The spatial term $f_b(\delta_i, E_i)$ for the background is considered to be independent of the right ascension α . Indeed, the ANTARES data set has been obtained by accumulating fifteen years of quasi-continuous measurement, therefore the non-uniformity of the detector exposure in local coordinates is averaged out by the rotation of the Earth, leading to a flat right ascension distribution of events. In practice, the value of the background spatial term $f_b(\delta_i, E_i)$ is estimated by a linear interpolation within a two-dimensional $(\sin \delta, E)$ histogram built from Monte Carlo simulations.

The spatial signal term is obtained by summing over all the individual blazars contributions:

$$f_s(\alpha_i, \delta_i, \beta_i, E_i) = \frac{1}{\sum w_j} \sum_{j=1}^{N_{\text{sources}}} w_j \mathcal{F}(\Psi_{ij}, \delta_i, \beta_i, E_i) \quad w_j = w_j^{\text{model}} \mathcal{A}(\delta_j), \quad (4)$$

where $\mathcal{F}(\Psi_{ij}, \delta_i, \beta_i, E_i)$ is the ANTARES point spread function (PSF) for track-like events, defined as the probability density for the event direction to fall within a given angular distance from the true incoming direction. The PSF is a sharply decreasing function of the space angle Ψ_{ij} between the i^{th} neutrino and the j^{th} blazar, and mostly depends, by decreasing order of importance, on the angular error β , the reconstructed energy E , and the declination δ . The practical implementation of the PSF is obtained from Monte Carlo simulations, by building two-dimensional histograms in (E, β) for 8 separate bins of $\sin \delta$.

The weight of the j^{th} blazar is proportional to its measured flux density $w_j^{\text{model}} = S_{8\text{GHz}}$, and corrected by the declination-dependent acceptance $\mathcal{A}(\delta)$ of the ANTARES neutrino track sample (computed for the particular $E^{-\gamma}$ energy spectrum considered). For comparison, a basic scenario where all blazars have the same weight, $w_j^{\text{model}} = 1$, is considered.

The smallest p -value obtained with the time-integrated likelihood analysis is $p = 2.6 \times 10^{-2}$ (2.2σ), for a $E^{-2.3}$ neutrino energy spectrum and with the radio-flux weight hypothesis. This spectral index value corresponds to the best-fit one from the ANTARES diffuse analysis [2], providing a hint that the VLBI blazars could contribute to the astrophysical neutrino diffuse flux. In comparison, when assuming an equal weight for each blazar in the likelihood, the resulting p -values ranges from $p = 7.6 \times 10^{-2}$ (1.8σ) for $E^{-2.3}$ up to $p = 0.38$ (0.9σ) for $E^{-1.8}$. The fact that smaller p -values are obtained with the flux-weight hypothesis could be an indication that the neutrino candidates correlate with blazars having a high flux density.

As the studied spatial correlation between neutrino candidates and the VLBI blazars is not statistically significant, upper limits (UL) at 90% confidence level are reported in Figure 4. The upper limits are computed for the different spectral indices of the assumed power-law neutrino flux (thin magenta lines), and their highest values as a function of the energy provides the most conservative limit curve (black dashed curve in the Figure). For comparison, the 68% allowed values from the ANTARES diffuse analysis are plotted (with a 15% systematic on the flux normalization included as in [56]), together with results from IceCube [57].

As mentioned at the beginning of this section, our best fit for a cosmic diffuse neutrino flux (orange dotted line) has a spectral index of $\gamma = 2.3$, and can be compared to the corresponding blazar upper limit (dotted magenta line). For this particular value of γ , the ratio of the magenta and orange dotted lines is ~ 0.2 , implying that the VLBI blazars could not contribute to more than $\sim 20\%$ of our estimated total diffuse flux of cosmic neutrinos. However, as can be seen on Figure 4, when accounting for the 68% confidence interval on the ANTARES diffuse flux estimation, the total VLBI upper-limit (black line) only weakly constrains our measurement. The

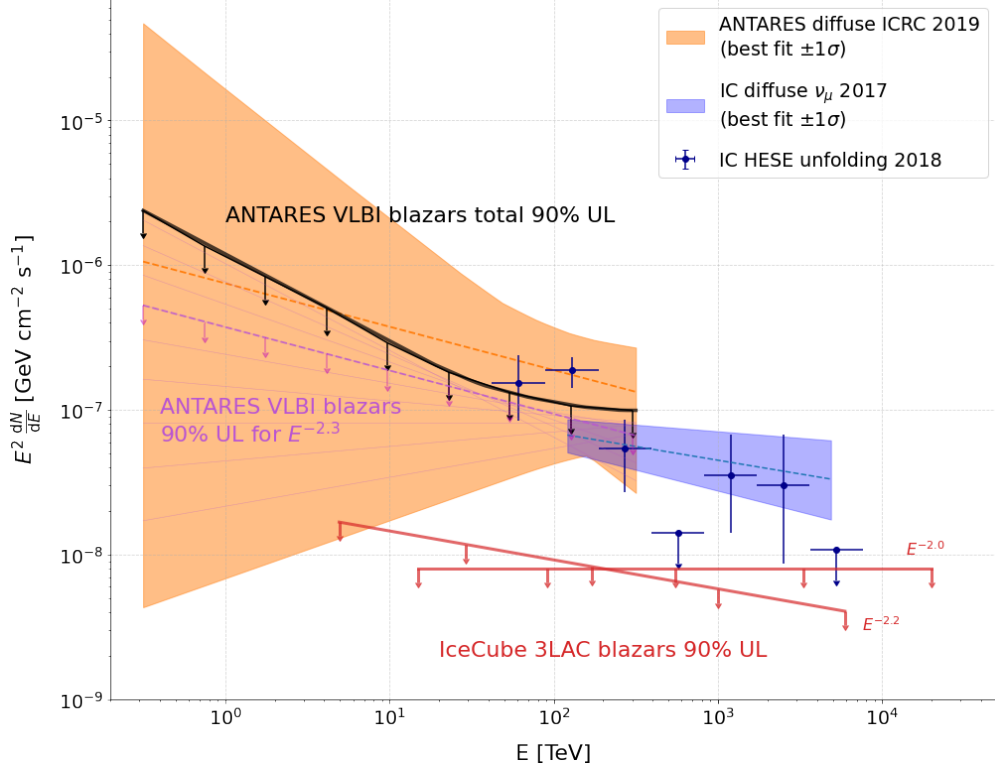


Figure 4: Upper limits on the one-flavour ($\nu_\mu + \bar{\nu}_\mu$) total neutrino flux from the VLBI blazars obtained with the time-integrated likelihood analysis as a function of the neutrino energy. The ANTARES limits for each of the spectral indices tested are represented by thin solid violet lines. For comparison, the IceCube limits [57] on *Fermi* 3LAC blazars for $E^{-2.0}$ and $E^{-2.2}$ spectra are shown in red. The thick black line shows the highest values of the single spectral index limits, and provides the most conservative upper-limit curve. For comparison, the orange-shaded band shows the 68% confidence region for the diffuse flux measured by ANTARES [2], the IceCube best fit to the astrophysical diffuse muon neutrino flux from [58] is displayed as a blue-shaded band, and the IceCube HESE spectrum from [59] is shown as blue markers.

total neutrino upper limit mildly constrains the first data point (blue marker) above 100 TeV of the IceCube HESE measurement, where the VLBI blazars would contribute $\sim 50\%$ of the flux.

6 Time-dependent likelihood scan

The time-dependent scan looks for neutrino flares from the direction of the selected radio-bright blazars and also relies on an unbinned maximum likelihood method. Since this search looks for clustering of events in space and time, the knowledge of the detection time of the selected events is included in the likelihood and combined with the spatial and energy information. This is achieved by multiplying the signal and background PDFs of Equation 3 by a time-dependent term. Unlike in the time-integrated analysis, the likelihood is maximised independently at the position of each investigated source, meaning that each source is analysed separately. Therefore, the spatial

signal term of Equation 4 simplifies into $f_s(\alpha_i, \delta_i, \beta_i, E_i) = \mathcal{F}(\Psi_{ij}, \delta_i, \beta_i, E_i)$. Regarding the signal time PDFs, two generic time profiles describing a temporary increase in neutrino emission – a Gaussian profile and a box profile – are tested. They are defined as:

$$\mathcal{S}_{\text{Gaussian}}^{\text{time}}(t_i) = \frac{1}{\sqrt{2\pi}\sigma_t} e^{-\frac{(t_i - T_0)^2}{2\sigma_t^2}}, \quad \mathcal{S}_{\text{box}}^{\text{time}}(t_i) = \begin{cases} \frac{1}{2\sigma_t}, & \text{if } [T_0 - \sigma_t] \leq t_i \leq [T_0 + \sigma_t]; \\ 0, & \text{otherwise;} \end{cases}, \quad (5)$$

with t_i being the detection time of the neutrino candidate event i , and T_0 and σ_t being the unknown central time and duration of the flaring emission, respectively, both fitted in the likelihood maximisation. Given the small expected contribution of a cosmic signal in the overall data set, the background time profile is built using the time distribution of data events, ensuring a time profile proportional to the measured data. This PDF is computed applying less stringent selection criteria than those of the final sample so as to avoid statistical fluctuations, using the same approach as in [60].

At the location of each investigated source, the likelihood is maximised leaving as free parameters the number of signal events μ_s , the signal spectral index γ , the central time of the flare T_0 , and the flare duration σ_t . The procedure allows for a single flare per blazar to be fitted, and, for the given best-fit flare (flare with highest Q), provides the best-fit values $\hat{\mu}_s$, $\hat{\gamma}$, \hat{T}_0 , $\hat{\sigma}_t$. In the maximisation, the spectral index can take values between 1.0 and 3.5. The range includes the value predicted by the candidate acceleration mechanism ($\gamma = 2.0$) and the softer best-fit spectral indices measured by the IceCube Collaboration for the diffuse neutrino flux ($\gamma = 2.37$ [61], $\gamma = 2.53$ [62]) and for the point-like sources showing evidence for neutrino emission, TXS 0506+056 ($\gamma = 2.1$ and $\gamma = 2.2$ [4]) and NGC 1068 ($\gamma = 3.2$ [6]). Concerning the time-dependent parameters, T_0 can vary over the time range of the investigated ANTARES data (from January 29, 2007 until February 29, 2020), while σ_t can take values between 1 day and 2000 days.

The test statistic Q , similarly to the time-integrated analysis, is defined as the logarithm of the ratio between the likelihood evaluated with the best-fit values of the free parameters and the background-only likelihood. However, in this case, the likelihood ratio is multiplied by a penalty term for short flares, $\frac{\hat{\sigma}_t}{\Delta T}$, with ΔT being the allowed time range for T_0 . The purpose of the penalty term is to account for the larger trial factor that should be associated to short flares since a larger number of short flares than of long ones can be accommodated in a given time range, as described in [63].

In order to estimate the p -value of the best flare for each investigated source, the observed Q -value is compared to the test statistic distribution obtained with background-only pseudo-experiments (PEs). Each PE is obtained using sets of data randomised in right ascension to eliminate any local clustering due to potential sources keeping the corresponding source declination. In particular, the p -value is given by the fraction of background-like PEs with a value of the test statistic larger than the observed Q . The lowest obtained p -value identifies the most significant flare of the search. Finally, a trial correction that accounts for the fact that many candidates have been investigated is applied, by comparing the lowest obtained p -value to the distribution of the smallest p -values found when performing the same analysis on many background-only PEs.

Figure 5 shows the expected performance of this approach compared to that of the time-integrated analysis, i.e. when the time information of the events is not considered. The 5σ discovery potential $\langle n_s^{5\sigma} \rangle$ – defined as the mean number of injected signal events needed for a 5σ discovery in 50% of the PEs – is shown as a function of the duration of the flare. The time-dependent search performs better along almost all the investigated range of flare durations, with an improvement in the discovery potential by a factor ~ 2 achieved for flares as short as 1 day.

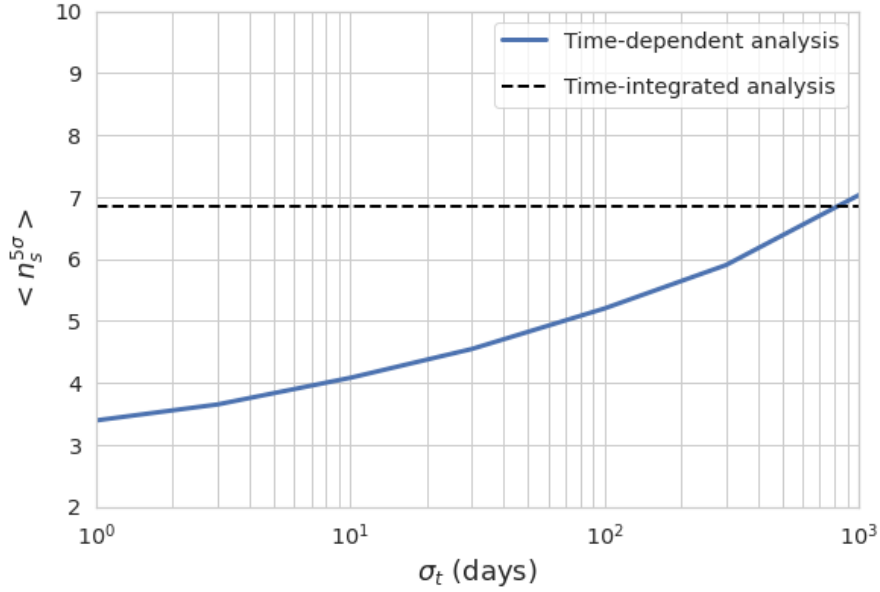


Figure 5: 5σ discovery potential in terms of mean number of signal events as a function of the simulated flare duration for the time-integrated analysis (dashed) and for the time-dependent analysis (solid). The simulated source is at a declination of $\delta = -40^\circ$ and the flare is centred at T_0 [MJD] = 57000. Similar results are obtained for different source declinations and central times.

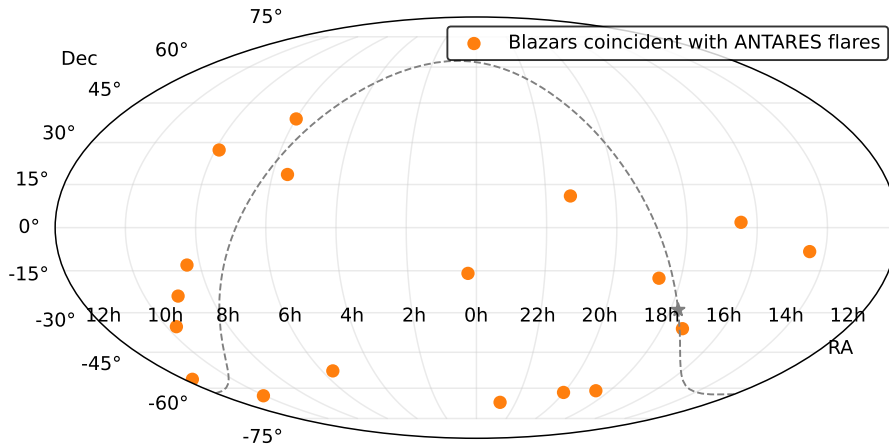


Figure 6: Sky map in equatorial coordinates showing the positions of the VLBI blazars coincident with the 3σ -flares found in ANTARES data (orange dots). See Table 1 for a list of these flares. The location of the Galactic plane (dashed line) and of the Galactic Center (star marker) is also shown.

The search results in 18 sources showing a flare with a pre-trial significance above 3σ for at least one of the tested time profiles. They are visualized in Figure 6 and listed in Table 1, together with the corresponding best-fit values of the free parameters. The most significant

Table 1: List of radio-bright blazars for which a pre-trial significance above 3σ for at least one of the tested time profiles (Gaussian-shaped and box-shaped) has been obtained. The first three columns report the name and equatorial coordinates of the sources. The remaining columns summarise the results of the search in terms of best-fit central time of the flare \hat{T}_0 , flare duration $\hat{\sigma}_t$, number of signal events $\hat{\mu}_s$, spectral index $\hat{\gamma}$ and pre-trial p -value, for the Gaussian-shaped and box-shaped signal time profile. The most significant flare found assuming each of the considered time shape is highlighted in bold.

Source			Results									
Name	δ	α	Gaussian-shaped time profile					Box-shaped time profile				
	[deg]	[deg]	\hat{T}_0	$\hat{\sigma}_t$	$\hat{\mu}_s$	$\hat{\gamma}$	p -value	\hat{T}_0	$\hat{\sigma}_t$	$\hat{\mu}_s$	$\hat{\gamma}$	p -value
			[MJD]	[days]				[MJD]	[days]			
J0112–6634	–66.6	18.1	58215	304	4.5	2.7	0.0026	58154	305	3.8	2.7	0.0097
J1355–6326	–63.4	208.9	56524	1041	7.9	2.8	0.00018	56091	905	6.0	2.9	0.0048
J0359–6154	–61.9	59.7	56316	78	5.4	3.5	0.0022	56321	112	5.7	3.5	0.0013
J0522–6107	–61.1	80.6	56221	42	4.6	3.4	0.0034	56232	59	4.9	3.4	0.0023
J1220–5604	–56.1	185.1	58406	18	2.8	2.6	0.00029	58413	22	0.4	2.2	0.0032
J1825–5230	–52.5	276.3	57265	600	5.4	2.7	0.0031	57188	959	5.5	2.7	0.0027
J0641–3554	–35.9	100.3	58084	16	2.9	3.0	0.0021	58081	19	3.0	3.0	0.0018
J1418–3509	–35.2	214.7	58120	11	3.3	2.9	0.0018	58121	14	2.9	2.8	0.0021
J1500–2358	–24.0	225.2	55846	4	3.7	2.3	0.0016	55847	6	3.7	2.2	0.0015
J0521–1737	–17.6	80.3	57332	1	2.0	1.9	0.0011	57333	1	2.0	1.9	0.0023
J2345–1555	–15.9	356.3	57653	460	3.2	2.6	0.0011	57784	404	2.4	2.7	0.0030
J1537–1259	–13.0	234.3	58201	46	2.6	2.0	0.0019	58201	55	2.7	2.0	0.0016
J0933–0819	–8.3	143.3	57411	533	3.1	2.0	0.0014	57128	697	2.9	2.0	0.0017
J0732+0150	1.8	113.1	55794	82	5.0	3.5	0.0010	55854	61	2.7	3.4	0.033
J0242+1101	11.0	40.6	56676	311	5.4	2.2	0.0060	56586	451	6.6	2.6	0.0021
J1826+1831	18.5	276.6	57672	151	2.9	2.5	0.0015	57636	178	3.0	2.5	0.0010
J1606+2717	27.3	241.7	58793	1	1.0	1.0	0.00076	58793	1	1.0	1.0	0.0017
J1800+3848	38.8	270.1	56590	3	1.7	2.4	0.0024	56590	3	1.9	2.6	0.0021

Gaussian (box) flare is found from the direction of J1355–6326 (correspondingly, J1826+1831), with a pre-trial significance of 3.7σ (correspondingly, 3.3σ) in the two-sided convention. When accounting for the fact that multiple sources have been investigated, a post-trial p -value of 29% and 84% is obtained for the best Gaussian and box flares, respectively. The weighted time distribution of the ANTARES events close to J1355–6326 and J1826+1831 is shown in Figure 7. Only track-like (shower-like) events within a distance of 5° (10°) from the blazars are included in the plot. A higher weight is associated to events with smaller distance to the source and larger value of the energy estimator.

While none of the investigated sources alone is observed at a significant detection level when accounting for trials, a further study is performed to check for the presence of a cumulative excess. By performing background PEs in which the same source catalog is targeted, it is found, as shown in Figure 8, that the probability to find 18 or more sources with a pre-trial significance greater than 3σ is 1.4% (2.5σ). This result provides an additional hint to the time-independent analysis, that a fraction of the blazars contained in the VLBI catalog could be neutrino emitters.

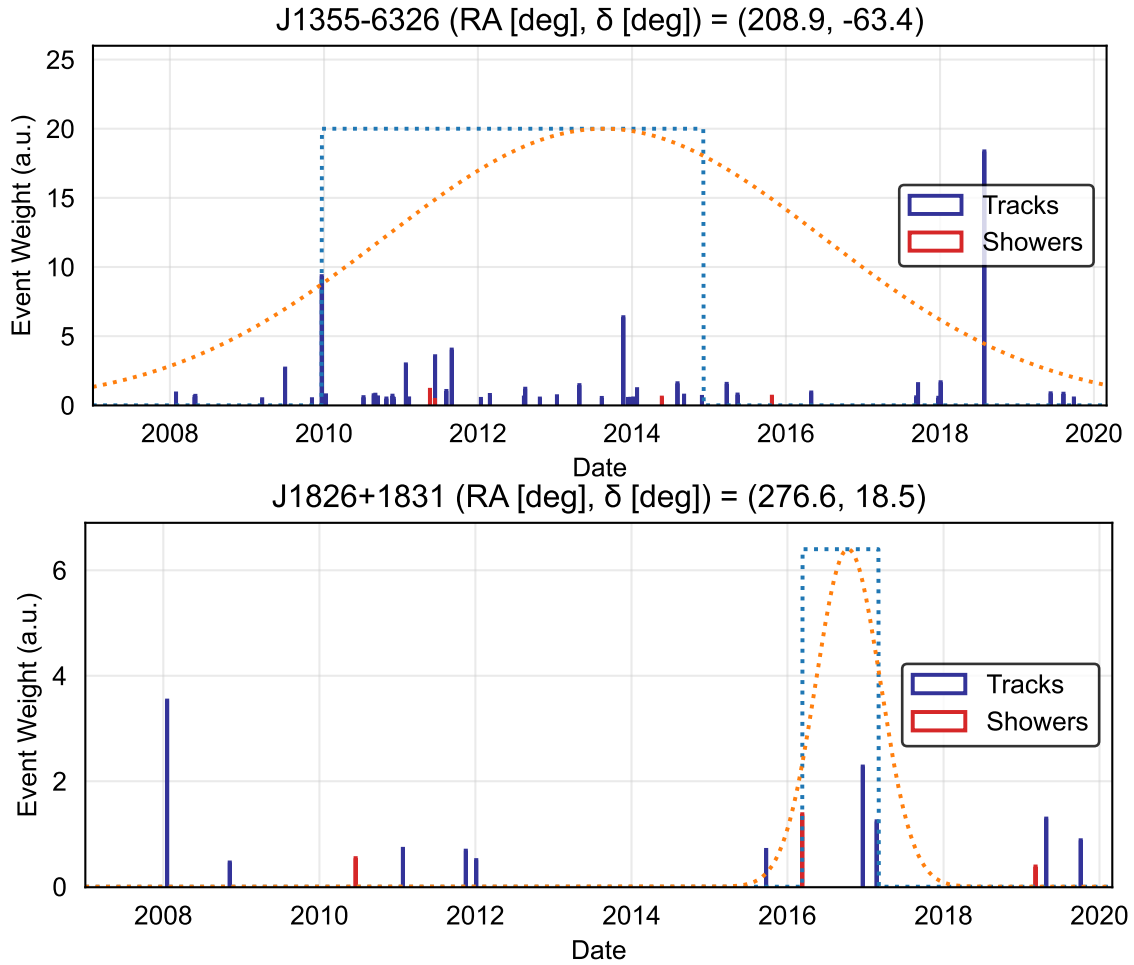


Figure 7: Weighted time distribution of the ANTARES events close to the location of J1355–6326 (top) and J1826+1831 (bottom). The dotted box and Gaussian time profiles have been drawn using the best-fit values of $\hat{\sigma}_t$ and \hat{T}_0 found in each case and reported in Table 1. Tracks (showers) are shown in blue (red).

7 Multi-messenger flares comparison

As a follow-up study of the findings of this analysis, the obtained best-fit neutrino flares have been compared to the radio light curves produced by the Owens Valley Radio Observatory (OVRO) [64] for those sources of Table 1 for which radio data are available. A notable overlap in time is noticed between the best-fit neutrino flare found in this analysis from the direction of J0242+1101 (PKS 0239+108) and its largest flare observed in radio, as shown in Figure 9. In view of this observation, the time distribution of the public data of the *Fermi* LAT γ -ray telescope and of the IceCube neutrino telescope compatible with the direction of J0242+1101 have also been studied. Figure 9 reports also the adaptive binned γ -ray light curve, obtained from *Fermi* data using the method described in [65, 66]. Remarkably, the most significant *Fermi* γ -ray flare for this blazar happened during the flaring emission detected in radio and the period

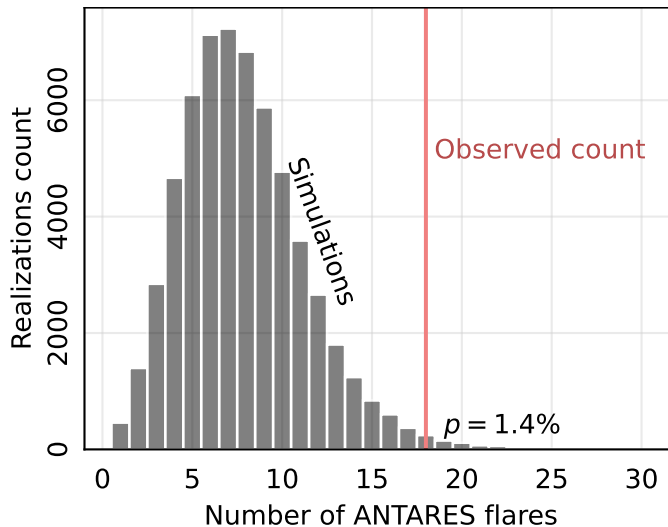


Figure 8: Cumulative excess of 3σ -flares found in ANTARES data. The vertical line indicates the observed count, while the histogram represents the number of sources in random realizations. The probability to observe 18 or more sources with a pre-trial flare significance above 3σ is 1.4%.

highlighted by the ANTARES analysis. Note that the γ -ray flare peak preceding radio is a typical scenario explained by synchrotron self-absorption of the jet base; this locates the γ -ray emission region close to the jet base [67, 66]. The time distribution of the IceCube track-like events in the 10-year point-source sample [68] with direction compatible with the blazar position within the 50% angular error reported by the IceCube Collaboration, is also shown. Only events with an angular uncertainty contour smaller than 10 deg^2 are depicted. While there is no evidence of time clustering of the IceCube events, a ν_μ -induced track with the notable high energy of 50 TeV was detected during the flare, its reported angular uncertainty radius being 1.4° . Furthermore, it is worth reporting that three IceCube alerts [69], namely 131165:9342044, 129933:32926212, and 128672:38561326, have a likelihood best-fit direction which lies at a distance of 1.4° , 1.5° , and 1.6° , respectively, from J0242+1101. However, their detection date is subsequent to the one of the flare discussed here.

The neutrino-radio- γ flare coincidence in J0242+1101 is an *a-posteriori* non-blind finding. It is still instructive to evaluate how likely such a correlation is to arise by chance. This study is conducted by running the whole flare fitting pipeline on background-only PEs. Each simulation of the analysis results in a fake list of neutrino flares, similar to Table 1. Then, exactly the same calculations are performed for the real list of flares and for random realizations. Specifically, blazars with the following characteristics are counted:

- the global maximum of their radio/ γ light curve falls within the ANTARES flare duration, $\hat{T}_0 \pm \hat{\sigma}_t$;
- that maximum is at least as high as for J0242+1101, compared to the median flux of the same blazar; this corresponds to maximum-to-median ratios above 1.6 for radio, and above 3.5 for γ .

Thanks to OVRO and *Fermi* observatories, both radio and γ -ray light curves are available for hundreds of blazars: the CGRaBS OVRO sample [27] and weekly curves from the *Fermi* LAT

light Curve Repository³ [70]. There are 335 blazars in the intersection of these samples.

The outcome of this study indicates that it is relatively rare to find even a single matching blazar with the above mentioned characteristics: it appears in only $p = 0.5\%$ of random realizations; 4% for either radio or γ -rays separately. This fraction of $p = 0.5\%$ is the p -value, the chance coincidence probability to observe this kind of temporal neutrino-electromagnetic correlation. Given that the J0242+1101 analysis is *a-posteriori*, these findings should be considered as hints to be tested further when more data become available.

8 Summary

A search for associations between 3411 radio-bright blazars of a complete VLBI-flux-density limited all-sky sample, and an ANTARES neutrino event sample has been performed.

A time-integrated association search was conducted with pair-counting and likelihood-based approaches, using only the track-like neutrino candidates. The pair-counting method finds an excess of 59 neutrino-blazar pairs, with post-trial p -value of 0.03 (2.2σ). The likelihood-based method finds a similar p -value of $p = 0.03$, for an energy spectrum of $E^{-2.3}$ and with the assumption of a neutrino flux proportional to the VLBI flux density. Upper limits on the neutrino flux from VLBI blazars are computed for different values of the spectral index $E^{-\gamma}$, mildly constraining the IceCube HESE measurement around 100 TeV, where the VLBI blazars would contribute to $\sim 50\%$ of the flux.

The time-dependent search for flares, conducted using an unbinned maximum likelihood method and combining track-like and shower-like samples, finds 18 sources with neutrino flares above 3σ (pre-trial). The two most significant flares come from the blazars J1355–6326 (3.7σ) and J1826+1831 (3.3σ), see Table 1. However, neither is significant alone after correcting for multiple trials. A cumulative effect is detected with $p = 0.014$ (2.5σ). This could be a hint of a population of blazars producing neutrinos with strong variations of the flux density.

A notable temporal correspondence between the neutrino flare from the direction of the J0242+1101 blazar, and the most prominent wide-band electromagnetic flare of that source is found. The chance probability of such a coincidence between neutrino emission, radio, and γ -ray light curves is $p = 0.5\%$. This is a *post-hoc* estimate that could be a hint for a connection between neutrino and electromagnetic emission. More observational data are required to verify the correlation more robustly and look for other similar coincidences.

The first results on associating ANTARES neutrinos with radio-bright blazars are presented in this paper. Blazar neutrino emission appears highly variable and is likely to correlate with electromagnetic flares. Still, the situation is far from being clear, other classes of neutrino sources should contribute: the neutrino sky can be diverse, including a Galactic component. All neutrino observatories, IceCube, KM3NeT, and Baikal-GVD, are continuously improving to provide more detections with better directional accuracy and reliability. A strengthening of the observed correlation between blazars and neutrinos could then be expected in the coming years. Radio observational programs are ongoing to aid in reliable identification of coincidences and better understanding of associations.

³<https://fermi.gsfc.nasa.gov/ssc/data/access/lat/LightCurveRepository/>

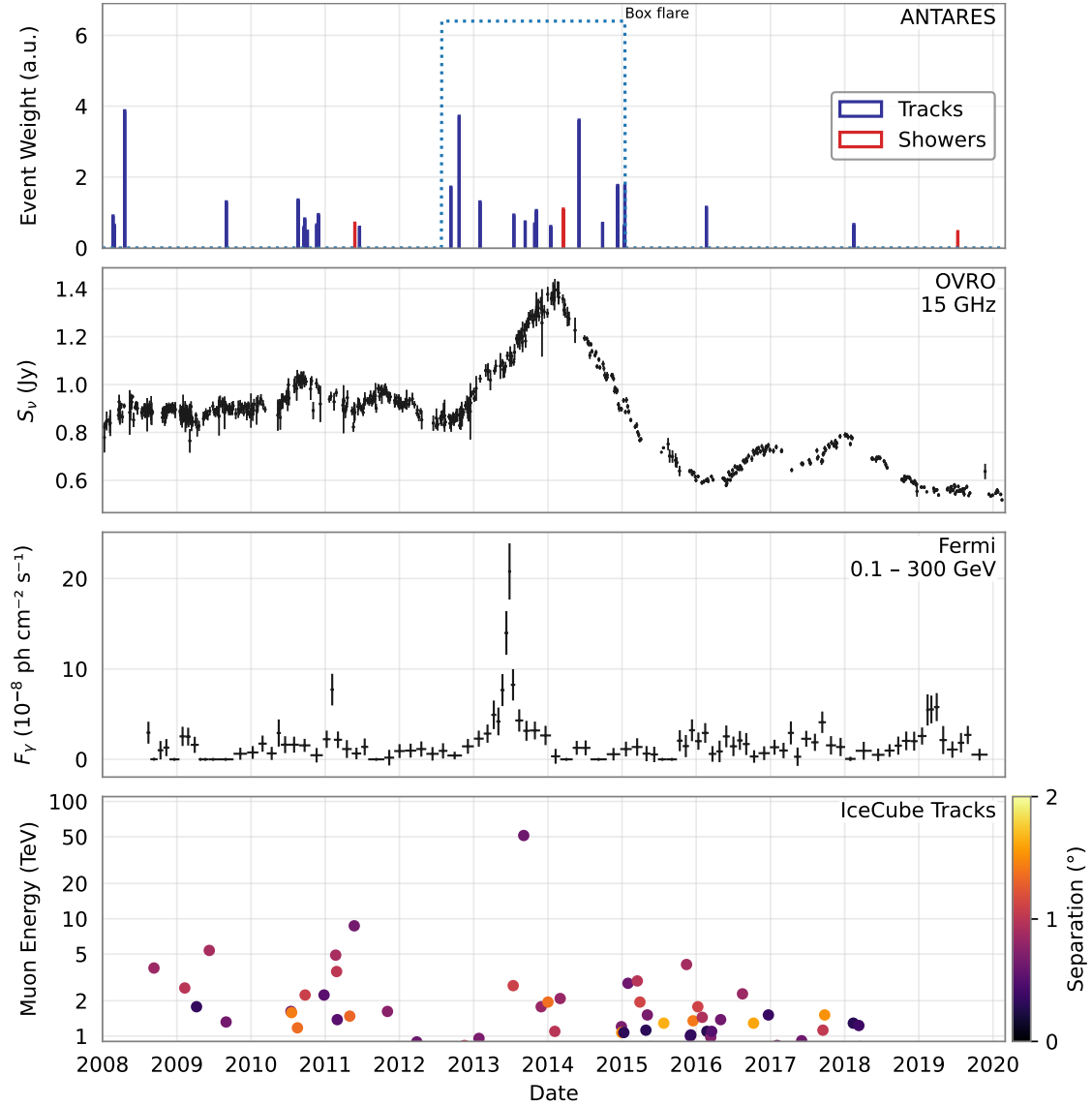


Figure 9: Multi-messenger light curves from the direction of the blazar J0242+1101 as a function of time, since 2008. Top panel: weighted time distribution of the ANTARES track-like (shower-like) events within 5° (10°) from this object. The box profile has been drawn using the best-fit values of $\hat{\sigma}_t$ and \hat{T}_0 found in this analysis. Second panel: OVRO radio light curve. Third panel: adaptive binned γ -ray light curve obtained from *Fermi* LAT data. Bottom panel: weighted time distribution of the IceCube track-like events closer to J0242+1101 than their 50% angular uncertainty. The applied weight corresponds to the energy of each event. The color scale indicates the event angular distance from the source.

Acknowledgements

We thank Eduardo Ros for helpful comments on the manuscript. This research has made use of data from the OVRO 40-m monitoring program, supported by private funding from the California

Institute of Technology and the Max Planck Institute for Radio Astronomy, and by NASA grants NNX08AW31G, NNX11A043G, and NNX14AQ89G and NSF grants AST-0808050 and AST-1109911.

The authors acknowledge the financial support of the funding agencies: Centre National de la Recherche Scientifique (CNRS), Commissariat à l'énergie atomique et aux énergies alternatives (CEA), Commission Européenne (FEDER fund and Marie Curie Program), LabEx UnivEarthS (ANR-10-LABX-0023 and ANR-18-IDEX-0001), Région Alsace (contrat CPER), Région Provence-Alpes-Côte d'Azur, Département du Var and Ville de La Seyne-sur-Mer, France; Bundesministerium für Bildung und Forschung (BMBF), Germany; Istituto Nazionale di Fisica Nucleare (INFN), Italy; Nederlandse organisatie voor Wetenschappelijk Onderzoek (NWO), the Netherlands; Executive Unit for Financing Higher Education, Research, Development and Innovation (UEFISCDI), Romania; Grants PID2021-124591NB-C41, -C42, -C43 funded by MCIN/AEI/10.13039/501100011033 and, as appropriate, by "ERDF A way of making Europe", by the "European Union" or by the "European Union NextGenerationEU/PRTR", Programa de Planes Complementarios I+D+I (refs. ASFAE/2022/023, ASFAE/2022/014), Programa Prometeo (PROMETEO/2020/019) and GenT (refs. CIDEAGENT/2018/034, /2019/043, /2020/049. /2021/23) of the Generalitat Valenciana, EU: MSC program (ref. 101025085), Spain; Ministry of Higher Education, Scientific Research and Innovation, Morocco, and the Arab Fund for Economic and Social Development, Kuwait. We also acknowledge the technical support of Ifremer, AIM and Foselev Marine for the sea operation and the CC-IN2P3 for the computing facilities. Y. Y. K. acknowledges support from the M2FINDERS project which has received funding from the European Research Council (ERC) under the European Union's Horizon 2020 Research and Innovation Programme (grant agreement No. 101018682). T. H. was supported by the Academy of Finland projects 317383, 320085, 322535, and 345899. S. K. acknowledges support from the European Research Council (ERC) under the European Unions Horizon 2020 research and innovation programme under grant agreement No. 771282.

References

- [1] M. G. Aartsen *et al.* (IceCube Collaboration), “Observation of High-Energy Astrophysical Neutrinos in Three Years of IceCube Data,” *Phys. Rev. Lett.* **113** (2014) 101101, [arXiv:1405.5303 \[astro-ph.HE\]](#).
- [2] L. A. Fusco and F. Versari (ANTARES Collaboration), “Study of the high-energy neutrino diffuse flux with the ANTARES neutrino telescope,” *PoS ICRC2019* (2020) 891.
- [3] V. A. Allakhverdyan *et al.* (Baikal-GVD Collaboration), “Diffuse neutrino flux measurements with the Baikal-GVD neutrino telescope,” *Phys. Rev. D* **107** no. 4, (2023) 042005, [arXiv:2211.09447 \[astro-ph.HE\]](#).
- [4] M. G. Aartsen *et al.* (IceCube Collaboration), “Neutrino emission from the direction of the blazar TXS 0506+056 prior to the IceCube-170922A alert,” *Science* **361** no. 6398, (2018) 147–151, [arXiv:1807.08794 \[astro-ph.HE\]](#).
- [5] M. G. Aartsen *et al.* (IceCube, Fermi-LAT, MAGIC, AGILE, ASAS-SN, HAWC, H.E.S.S., INTEGRAL, Kanata, Kiso, Kapteyn, Liverpool Telescope, Subaru, Swift NuSTAR, VERITAS, VLA/17B-403 Collaboration), “Multimessenger observations of a flaring blazar coincident with high-energy neutrino IceCube-170922A,” *Science* **361** no. 6398, (2018) eaat1378, [arXiv:1807.08816 \[astro-ph.HE\]](#).
- [6] R. Abbasi *et al.* (IceCube Collaboration), “Evidence for neutrino emission from the nearby active galaxy NGC 1068,” *Science* **378** no. 6619, (2022) 538–543, [arXiv:2211.09972 \[astro-ph.HE\]](#).
- [7] A. Plavin *et al.* “Observational Evidence for the Origin of High-energy Neutrinos in Parsec-scale Nuclei of Radio-bright Active Galaxies,” *Astrophys. J.* **894** no. 2, (2020) 101, [arXiv:2001.00930 \[astro-ph.HE\]](#).
- [8] A. Plavin *et al.* “Directional Association of TeV to PeV Astrophysical Neutrinos with Radio Blazars,” *Astrophys. J.* **908** no. 2, (2021) 157, [arXiv:2009.08914 \[astro-ph.HE\]](#).
- [9] A. Plavin *et al.* “Growing evidence for high-energy neutrinos originating in radio blazars,” *Mon. Not. Roy. Astron. Soc.* **523** no. 2, (2023) 1799–1808, [arXiv:2211.09631 \[astro-ph.HE\]](#).
- [10] E. Kun *et al.* “Multiwavelength Search for the Origin of IceCube’s Neutrinos,” *Astrophys. J.* **934** no. 2, (2022) 180, [arXiv:2203.14780 \[astro-ph.HE\]](#).
- [11] S. Buson *et al.* “Beginning a Journey Across the Universe: The Discovery of Extragalactic Neutrino Factories,” *Astrophys. J. Lett.* **933** no. 2, (2022) L43, [arXiv:2207.06314 \[astro-ph.HE\]](#). [Erratum: *Astrophys.J.Lett.* 934, L38 (2022), Erratum: *Astrophys.J.* 934, L38 (2022)].
- [12] P. Giommi *et al.* “Dissecting the regions around IceCube high-energy neutrinos: growing evidence for the blazar connection,” *Mon. Not. Roy. Astron. Soc.* **497** no. 1, (2020) 865–878, [arXiv:2001.09355 \[astro-ph.HE\]](#).
- [13] R. Abbasi *et al.* (IceCube Collaboration), “Constraints on Populations of Neutrino Sources from Searches in the Directions of IceCube Neutrino Alerts,” *Astrophys. J.* **951** no. 1, (2023) 45, [arXiv:2210.04930 \[astro-ph.HE\]](#).

- [14] S. Buson *et al.* “Extragalactic neutrino factories,” [arXiv:2305.11263](#) [astro-ph.HE].
- [15] A. Albert *et al.* (ANTARES Collaboration), “New constraints on all flavor Galactic diffuse neutrino emission with the ANTARES telescope,” *Phys. Rev. D* **96** no. 6, (2017) 062001, [arXiv:1705.00497](#) [astro-ph.HE].
- [16] A. Albert *et al.* (ANTARES, IceCube Collaboration), “Joint Constraints on Galactic Diffuse Neutrino Emission from the ANTARES and IceCube Neutrino Telescopes,” *Astrophys. J. Lett.* **868** no. 2, (2018) L20, [arXiv:1808.03531](#) [astro-ph.HE].
- [17] A. Albert *et al.* (ANTARES Collaboration), “Hint for a TeV neutrino emission from the Galactic Ridge with ANTARES,” *Phys. Lett. B* **841** (2023) 137951, [arXiv:2212.11876](#) [astro-ph.HE].
- [18] A. Neronov and D. V. Semikoz “Evidence the Galactic contribution to the IceCube astrophysical neutrino flux,” *Astropart. Phys.* **75** (2016) 60–63, [arXiv:1509.03522](#) [astro-ph.HE].
- [19] M. G. Aartsen *et al.* (IceCube Collaboration), “Search for Sources of Astrophysical Neutrinos Using Seven Years of IceCube Cascade Events,” *Astrophys. J.* **886** (2019) 12, [arXiv:1907.06714](#) [astro-ph.HE].
- [20] R. Abbasi *et al.* (IceCube Collaboration), “Observation of high-energy neutrinos from the Galactic plane,” *Science* **380** no. 6652, (2023) adc9818, [arXiv:2307.04427](#) [astro-ph.HE].
- [21] Y. Y. Kovalev *et al.* “Galactic Contribution to the High-energy Neutrino Flux Found in Track-like IceCube Events,” *Astrophys. J. Lett.* **940** no. 2, (2022) L41, [arXiv:2208.08423](#) [astro-ph.HE].
- [22] V. Berezhinsky “Extraterrestrial neutrino sources and high energy neutrino astrophysics,” in *Proceedings of the Neutrino-77 Conference, Moscow*, p. 177. 1977.
- [23] D. Eichler “High-energy neutrino astronomy: a probe of galactic nuclei?,” *Astrophys. J.* **232** no. 1, (1979) 106–112.
- [24] K. Murase “Active Galactic Nuclei as High-Energy Neutrino Sources,” *Neutrino Astronomy: Current Status, Future Prospects* (2017) 15–31, [arXiv:1511.01590](#) [astro-ph.HE].
- [25] M. Boettcher “Progress in Multiwavelength and Multi-Messenger Observations of Blazars and Theoretical Challenges,” *Galaxies* (2019) , [arXiv:1901.04178](#) [astro-ph.HE].
- [26] R. Blandford *et al.* “Relativistic Jets from Active Galactic Nuclei,” *ARA&A* **57** (Aug., 2019) 467–509, [arXiv:1812.06025](#) [astro-ph.HE].
- [27] T. Hovatta *et al.* “Association of IceCube neutrinos with radio sources observed at Owens Valley and Metsähovi Radio Observatories,” *Astron. Astrophys.* **650** (2021) A83, [arXiv:2009.10523](#) [astro-ph.HE].
- [28] S. Adrian-Martinez *et al.* (ANTARES Collaboration), “Search for muon-neutrino emission from GeV and TeV gamma-ray flaring blazars using five years of data of the ANTARES telescope,” *JCAP* **12** (2015) 014, [arXiv:1506.07354](#) [astro-ph.HE].

- [29] A. Albert *et al.* (ANTARES Collaboration), “ANTARES Search for Point Sources of Neutrinos Using Astrophysical Catalogs: A Likelihood Analysis,” *Astrophys. J.* **911** no. 1, (2021) 48, [arXiv:2012.15082 \[astro-ph.HE\]](#).
- [30] R. Abbasi *et al.* (IceCube Collaboration), “The IceCube high-energy starting event sample: Description and flux characterization with 7.5 years of data,” *Phys. Rev. D* **104** (2021) 022002, [arXiv:2011.03545 \[astro-ph.HE\]](#).
- [31] M. Boettcher *et al.* “Multiwavelength and Multimessenger Observations of Blazars and Theoretical Modeling: Blazars as Astrophysical Neutrino Sources,” *Acta Phys. Polon. Supp.* **15** no. 3, (2022) 8, [arXiv:2204.12242 \[astro-ph.HE\]](#).
- [32] R. Abbasi *et al.* (IceCube Collaboration), “IceCat-1: the IceCube Event Catalog of Alert Tracks,” [arXiv:2304.01174 \[astro-ph.HE\]](#).
- [33] R. Abbasi *et al.* (IceCube Collaboration), “Search for Correlations of High-energy Neutrinos Detected in IceCube with Radio-bright AGN and Gamma-Ray Emission from Blazars,” *Astrophys. J.* **954** no. 1, (2023) 75, [arXiv:2304.12675 \[astro-ph.HE\]](#).
- [34] M. Ajello *et al.* (Fermi-LAT Collaboration), “The Fourth Catalog of Active Galactic Nuclei Detected by the Fermi Large Area Telescope,” *Astrophys. J.* **892** (2020) 105, [arXiv:1905.10771 \[astro-ph.HE\]](#).
- [35] M. Ageron *et al.* (ANTARES Collaboration), “ANTARES: the first undersea neutrino telescope,” *Nucl. Instrum. Meth.* **A656** (2011) 11, [arXiv:1104.1607 \[astro-ph.IM\]](#).
- [36] A. Albert *et al.* (ANTARES Collaboration), “First all-flavor neutrino pointlike source search with the ANTARES neutrino telescope,” *Phys. Rev. D* **96** no. 8, (2017) 082001, [arXiv:1706.01857 \[astro-ph.HE\]](#).
- [37] L. Petrov *et al.* “Precise geodesy with the Very Long Baseline Array,” *Journal of Geodesy* **83** (2009) 859–876, [arXiv:0806.0167 \[physics.geo-ph\]](#).
- [38] A. B. Pushkarev and Y. Y. Kovalev “Single-epoch VLBI imaging study of bright active galactic nuclei at 2 GHz and 8 GHz,” *Astron. Astrophys.* **544** (2012) A34, [arXiv:1205.5559](#).
- [39] B. G. Piner *et al.* “Relativistic Jets in the Radio Reference Frame Image Database. II. Blazar Jet Accelerations from the First 10 Years of Data (1994-2003),” *Astrophys. J.* **758** (2012) 84, [arXiv:1208.4399](#).
- [40] A. J. Beasley *et al.* “The VLBA Calibrator Survey: VCS1,” *Astrophys. J. Suppl.* **141** (2002) 13–22, [arXiv:astro-ph/0201414](#).
- [41] E. B. Fomalont *et al.* “The Second VLBA Calibrator Survey: VCS2,” *Astron. J.* **126** (2003) 2562–2566.
- [42] L. Petrov *et al.* “The Third VLBA Calibrator Survey: VCS3,” *Astron. J.* **129** (2005) 1163–1170, [arXiv:astro-ph/0409698](#).
- [43] L. Petrov *et al.* “The Fourth VLBA Calibrator Survey: VCS4,” *Astron. J.* **131** (2006) 1872–1879, [arXiv:astro-ph/0508506](#).
- [44] Y. Y. Kovalev *et al.* “The Fifth VLBA Calibrator Survey: VCS5,” *Astron. J.* **133** (2007) 1236–1242, [arXiv:astro-ph/0607524](#).

- [45] L. Petrov *et al.* “The Sixth VLBA Calibrator Survey: VCS6,” *Astron. J.* **136** (2008) 580, [arXiv:0801.3895](#) [astro-ph].
- [46] L. Petrov “The Wide-field VLBA Calibrator Survey: WFCS,” *Astron. J.* **161** no. 1, (2021) 14, [arXiv:2008.09243](#) [astro-ph.IM].
- [47] D. Gordon *et al.* “Second Epoch VLBA Calibrator Survey Observations: VCS-II,” *Astron. J.* **151** no. 6, (2016) 154.
- [48] L. Petrov *et al.* “The Very Long Baseline Array Galactic Plane Survey—VGaPS,” *Mon. Notices Royal Astron. Soc.* **142** no. 2, (2011) 35, [arXiv:1101.1460](#) [astro-ph.CO].
- [49] L. Petrov “The Catalog of Positions of Optically Bright Extragalactic Radio Sources OBRS-1,” *Astron. J.* **142** no. 4, (2011) 105, [arXiv:1103.2840](#) [astro-ph.CO].
- [50] L. Petrov *et al.* “The LBA Calibrator Survey of southern compact extragalactic radio sources - LCS1,” *Mon. Notices Royal Astron. Soc.* **414** no. 3, (2011) 2528–2539, [arXiv:1012.2607](#) [astro-ph.CO].
- [51] L. Petrov “The EVN Galactic Plane Survey - EGaPS,” *Mon. Notices Royal Astron. Soc.* **419** no. 2, (2012) 1097–1106, [arXiv:1106.4883](#) [astro-ph.CO].
- [52] L. Petrov “The catalogue of positions of optically bright extragalactic radio sources OBRS-2,” *Astron. J.* **146** (2013) 5, [arXiv:1301.5407](#) [astro-ph.IM].
- [53] F. K. Schinzel *et al.* “New Associations of Gamma-Ray Sources from the Fermi Second Source Catalog,” *Astrophys. J. Suppl.* **217** no. 1, (2015) 4, [arXiv:1408.6217](#) [astro-ph.HE].
- [54] F. Shu *et al.* “VLBI Ecliptic Plane Survey: VEPS-1,” *Astrophys. J., Suppl. Ser.* **230** no. 2, (2017) 13, [arXiv:1701.07287](#) [astro-ph.IM].
- [55] L. Petrov *et al.* “The Second LBA Calibrator Survey of southern compact extragalactic radio sources - LCS2,” *Mon. Notices Royal Astron. Soc.* **485** no. 1, (2019) 88–101, [arXiv:1812.02916](#) [astro-ph.IM].
- [56] A. Albert *et al.* (ANTARES Collaboration), “All-flavor Search for a Diffuse Flux of Cosmic Neutrinos with Nine Years of ANTARES Data,” *Astrophys. J. Lett.* **853** no. 1, (2018) L7, [arXiv:1711.07212](#) [astro-ph.HE].
- [57] M. Huber “Searches for steady neutrino emission from 3FHL blazars using eight years of IceCube data from the Northern hemisphere,” *PoS ICRC2019 Madison* (2019) 916.
- [58] C. Haack and C. Wiebusch “A measurement of the diffuse astrophysical muon neutrino flux using eight years of IceCube data.,” *PoS ICRC2017 Busan* (2017) 1005.
- [59] C. Kopper “Observation of Astrophysical Neutrinos in Six Years of IceCube Data,” *PoS ICRC2017 Busan* (2017) 981.
- [60] A. Albert *et al.* (ANTARES Collaboration), “ANTARES neutrino search for time and space correlations with IceCube high-energy neutrino events,” *Astrophys. J.* **879** no. 2, (2019) 108, [arXiv:1902.09462](#) [astro-ph.HE].
- [61] R. Abbasi *et al.* (IceCube Collaboration), “Improved Characterization of the Astrophysical Muon-neutrino Flux with 9.5 Years of IceCube Data,” *Astrophys. J.* **928** no. 1, (2022) 50, [arXiv:2111.10299](#) [astro-ph.HE].

- [62] M. G. Aartsen *et al.* (IceCube Collaboration), “Characteristics of the diffuse astrophysical electron and tau neutrino flux with six years of IceCube high energy cascade data,” *Phys. Rev. Lett.* **125** no. 12, (2020) 121104, [arXiv:2001.09520](#) [astro-ph.HE].
- [63] J. Braun *et al.* “Time-dependent point source search methods in high energy neutrino astronomy,” *Astropart.Phys.* **33** no. 3, (2010) 175 – 181, [arXiv:0912.1572](#) [astro-ph.IM].
- [64] J. L. Richards *et al.* “Blazars in the Fermi Era: The OVRO 40 m Telescope Monitoring Program,” *Astrophys. J. Suppl.* **194** no. 2, (2011) 29, [arXiv:1011.3111](#) [astro-ph.CO].
- [65] B. Lott *et al.* “An adaptive-binning method for generating constant-uncertainty/constant-significance light curves with Fermi-LAT data,” *A&A* **544** (Aug., 2012) A6, [arXiv:1201.4851](#) [astro-ph.HE].
- [66] I. G. Kramarenko *et al.* “A decade of joint MOJAVE-Fermi AGN monitoring: localization of the gamma-ray emission region,” *MNRAS* **510** no. 1, (Feb., 2022) 469–480, [arXiv:2106.08416](#) [astro-ph.HE].
- [67] A. B. Pushkarev *et al.* “Radio/Gamma-ray Time Delay in the Parsec-scale Cores of Active Galactic Nuclei,” *ApJL* **722** no. 1, (Oct., 2010) L7–L11, [arXiv:1006.1867](#) [astro-ph.CO].
- [68] All-sky point-source IceCube data: years 2008-2018 <https://icecube.wisc.edu/data-releases/2021/01/all-sky-point-source-icecube-data-years-2008-2018/>
- [69] R. Abbasi *et al.* (IceCube Collaboration), “Constraints on Populations of Neutrino Sources from Searches in the Directions of IceCube Neutrino Alerts,” *Astrophys. J.* **951** no. 1, (2023) 45, [arXiv:2210.04930](#) [astro-ph.HE].
- [70] S. Abdollahi *et al.* (Fermi-LAT Collaboration), “The Fermi-LAT Lightcurve Repository,” *Astrophys. J. Suppl.* **265** no. 2, (2023) 31, [arXiv:2301.01607](#) [astro-ph.HE].